**PASJ:** Publ. Astron. Soc. Japan , 1–??,


# Multiple Component Analysis of Time Resolved Spectra of GRB041006: Clue to the Nature of Underlying Soft Component of GRB. (ver.080129b)

Yuji Shirasaki, [1] Atsumasa Yoshida, [2,4] Nobuyuki Kawai, [3,4] Toru Tamagawa, [4] Takanori Sakamoto, [5] Motoko Suzuki, [6] Yujin Nakagawa, [2] Akina Kobayashi, [2] Satoshi Sugita, [2,4] Ichiro Takahashi, [2] Makoto Arimoto, [3] Takashi Shimokawabe [3] Nicolas Vasquez Pazmino, [3] Takuto Ishimura, [3] Rie Sato, [7] Masaru Matsuoka, [6] Edward E. Fenimore, [8] Mark Galassi, [8] Donald Q. Lamb, [9] Carlo Graziani, [9] Timothy Q. Donaghy, [9] Jean-Luc Atteia, [10] Alexandre Pelangeon, [10] Roland Vanderspek, [11] Geoffrey B. Crew, [11] John P. Doty, [11] Joel Villasenor, [11] Gregory Prigozhin, [11] Nat Butler, [11,12] George R. Ricker, [11] Kevin Hurley, [12] Stanford E. Woosley, [13] and Graziella Pizzichini [14]

[1] *National Astronomical Observatory of Japan, Osawa, Mitaka, Tokyo, 181-8588*

[2] *Department of Physics and Mathematics, Aoyama Gakuin University, 5-10-1 Fuchinobe, Sagamihara, Kanagawa 229-8558*

[3] *Department of Physics, Tokyo Institute of Technology, 2-12-1 Ookayama, Meguro-ku, Tokyo 152-8551*
*arimoto@hp.phys.titech.ac.jp*

[4] *RIKEN, 2-1 Hirosawa, Wako Saitama 351-0198*

[5] *Goddard Space Flight Center, NASA, Greenbelt, Maryland, 20771, USA*

[6] *JAXA, 2-1-1 Sengen, Tsukuba, Ibaraki, 305-8505*

[7] *JAXA/ISAS, 3-1-1 Yoshinodai, Sagamihara, Kanagawa, 229-8510*

[8] *Los Alamos National Laboratory, P. O. ox 1663, Los Alamos, NM, 87545, USA*

[9] *Deparment of Astronomy and Astrophysics, University of Chicago, 5640 South Ellis Avenue, Chicago, Illinois 60637, USA*

[10] *LATT, Observatoire Midi-Pyrénées (CNRS-UPS), 14 Avenue E. Belin, 31400 Toulouse, France*

[11] *Center for Space Research, MIT, 77 Vassar Street, Cambridge, Massachusetts, 02139-4307, USA*

[12] *Space Sciences Laboratory, University of California , Berkeley, California, 94720-7450*

[13] *Department of Astronomy and Astrophysics, University of California at Sata Cruz, 477 Crark Kerr Hall, Santa Cruz, California, 95064, USA*

[14] *INAF/IASF Bologna, Via Gobetti 101, 40129 Bologna, Italy*

(Received 2008 0; accepted 2008 0)

**Abstract**

GRB 041006 was detected by HETE-2 at 12:18:08 UT on 06 October 2004. The GRB shows a soft X-ray emission, a precursor, before the onset of the main GRB, and also shows a soft X-ray tail after the end of the main peak. The light curves within four different energy bands show different features; At higher energy bands several peaks are seen in the light curve, while at lower energy band a single broader bump is dominated. It is expected that these different features are the result of mixture of several components each of which has different energetics and variability. To reveal the nature of each component, we analysed the time resolved spectra and they are successfully resolved into several components. We also found that these components can be classified into two distinct classes; One is a component which shows an exponential decay of $E_p$ with a characteristic time scale shorter than $\sim 30$ sec, and it spectrum is well represented by a broken power law function, which is frequently observed in many prompt GRB emissions, so it should be an internal-shock origin GRB. Another is a component whose $E_p$ is almost unchanged with characteristic time scale longer than $\sim 60$ sec, and shows a very soft emission and slower variability. The spectrum of the soft component is characterized by either a broken power law or a black body spectrum. So the component might originate from a relatively lower velocity jet or a photosphere of the fireball. By assuming that the soft component is a thermal emission, the radiation radius is initially $4.35^{+1.35}_{-1.05} \times 10^6$ km, which is a typical radius of a blue supergiant, ant its expansion velocity is $2.35 \times 10^5$ km/s at the source frame.

**Key words:** gamma-rays:busts — X-rays: bursts — X-rays: individual (GRB041006)

## 1. Introduction

On October 6, 2004 the High Energy Transient Explorer 2 (HETE-2) detected a GRB which shows a soft X-ray emission before the onset of the main GRB. Such a soft emission, a precursor, is predicted in some of theoretical models. The fireball undergoes a transition from an optically thick phase to an optically thin phase, then thermal radiation (fireball precursor) may occur during the transition (B. Paczynsky 1986 ,Daigne & Mochkovitch 2002 ). A precursor (progenitor precursor) may be emitted by the interaction of the jet with the progenitor star (Ramirez-Ruiz et al. 2002 ; Waxman & Mészáros 2003 ). The external shock by the first relativistic shell can also produce the non-thermal precursor (Umeda et al. 2005 ).

Soft precursors are occasionally detected in long GRBs. The first detection was made by the GINGA satellite (GRB 900126; Murakami et al. 1991 ). In the recent observations, BeppoSAX (e.g. GRB 011121; Piro et al. 2005 ), HETE2 (e.g. GRB 030329; Vanderspek et al. 2004) and Swift (e.g GRB 050820A; Cenko et al. 2006 , GRB 060124; Romona et al. 2006 , GRB 061121; Page et al. 2007 ) satellites also detected such a precursor event. Lazzati 2005 studied a bright long BATSE GRB light curve and found that in 20% of the cases there is evidence of a soft emission before the main GRB.

The precursor is usually detected as a single pulse that is well separated in time from the main GRB, typically several seconds to hundreds of seconds. The precursor of GRB 041006 is not well separated from the main GRB and is likely to be continuously active during the whole prompt GRB phase. Such a long lasting soft component was also observed in GRB 030329 (Vanderspek et al. 2004). Vetere et al. 2006 found that for some of the GRBs detected by BeppoSAX, there is a slowly varying soft component behind the highly variable main GRB. Borgonovo et al. 2007 analyzed the light curves obtained by BATSE, Konus and BeppoSAX, and found that the width of the auto-correlation function shows a remarkable bimodal distribution in the rest-frame of the source. This result suggests that there exists a slowly varying soft component in some GRBs. The relation among the underlying soft X-ray component, the X-ray precursor, and the main GRB is still open to question.

In this paper, we present the results on multiple component analysis of the time resolved spectra of GRB 041006.

## 2. Observation

The gamma-ray burst GRB 041006 was detected with the HETE FREGATE (Atteia et al. 2003) and the WXM (Shirasaki et al. 2003) instruments at 12:18:08 UT on 06 October 2004 (Galassi et al. 2004 ). The WXM flight software localized the burst in real time, resulting in a GCN Notice 42 seconds after the burst trigger. The flight error region was a circle of 14 arcminutes radius (90% confidence) centered at RA = 00h 54m 54s, DEC = +01d 18' 37" (J2000). Ground analyses of the burst data allow the error region to be refined to a circle of 5.0 arcminutes radius (90% confidence) centered at RA = 00h 54m 53s, DEC = +01d 12' 04" (J2000).

At 1.4 hour after the trigger, the optical afterglow was found by Costa et al. 2004 , and the redshift was first reported by Fugazza et al. 2004 and later confirmed by Price et al. 2004 to be $z = 0.716$. The follow-up observations were made at various observation sites (e.g. Urata et al. 2007) . The VLA observations were made but no radio sources were detected (Soderberg et al. 2004 ) The X-ray afterglow was found by Butler et al. 2005, which shows a power law decay with a slope of $-1.0 \pm 0.1$. The X-ray spectrum was characterized by an absorbed power law model with a photon index of $\Gamma = 1.9 \pm 0.2$ and $n_H = (1.1 \pm 0.5) \times 10^{21}$ cm$^{-2}$. The emergence of a supernova component was reported by Bikmaev et al. 2004 and Garg et al. 2004 . The field of GRB 041006 was imaged by Soderberg et al. 2005 using the WFC of the ACS onboard HST, and they found a SN 1998bw-like supernova dimmed by ∼0.3 magnitudes.

## 3. Analysis

The data obtained by the WXM and FREGATE instruments are reduced and calibrated with the standard manner. We use WXM TAG data and FREGATE PH data.

### *3.1. Temporal Properties*

Figure 1 shows the light curves of GRB 041006 for four energy bands with 0.5 sec time bins. $T_{50}$ and $T_{90}$ are measured for each energy band, and they are shown in Table 1.

The whole period of the burst can be divided into four major intervals accounting for a spectrum feature, and each major interval is divided into a few sub-intervals for time-resolved spectrum analysis. The time interval for each sub-interval is shown in Table 2. At the interval 1 soft emission showing no prominent activity above 40 keV is onset, then harder emissions are following in the interval 2 and 3. In the interval 4, the hard emission almost disappears and only a soft emission is gradually decaying.

We call the emission seen in the interval 1 as an X-ray precursor. The precursor shows a structured light curve in the lowest energy band (2∼10 keV), which indicates that two emissions are successively occurring. In the interval 2, two peaks are seen at the higher energy bands ($>$ 40 keV). The time history of the hardness ratio also clearly shows the corresponding peaks. At the lowest energy bands ($<$ 10 keV), such a structured emission is not clearly seen. In the interval 3, two harder peaks are seen at the highest energy band (80 ∼ 400 keV), and such a structure is blurred at the lower energy bands. The emission in the interval 4, which we call as an X-ray tail, shows no prominent structure.

From the dissimilarity of the light curves among the four energy bands, it is inferred that the total emission is composed of several independent emissions which have different characteristic energies. For examples, two components which contribute to the precursor, four compo-

nents seen as a peak in the energy band $40 \sim 80$ $keV$ and $80 \sim 400$ $keV$, and one broad soft component which constitutes the major part of the light curve in the lowest energy band. To investigate such hypothesis, we performed time resolved spectrum analysis based on a multiple-components spectrum model.

### *3.2. Average Spectrum Properties*

The joint spectral analysis of WXM and FREGATE data is performed using XSPEC v.11.3.1 (Arnaud 1996 ). The time integrated spectrum of GRB 041006 is approximately described by a broken power law function (Figure 2); The low energy photon index is $\alpha = 1.28 \pm 0.02$, the high energy index is $\beta = 2.14 \pm 0.07$, the peak energy is $E_p = 22.5 \pm 1.7$ keV and the flux at 1 keV is $K = 4.25 \pm 0.15$ cm$^{-2}$s$^{-1}$ keV$^{-1}$, where the quoted errors are in one sigma. The $\chi^2$ is 111.19 for 79 dof, and Null hypothesis probability is 0.0099, so the fitting is not so good. From this fitting result, we obtained $S_X = (5.24 \pm 0.08) \times 10^{-6}$ ergs cm$^{-2}$, $S_\gamma = (7.13 \pm 0.12) \times 10^{-6}$ ergs cm$^{-2}$, where $S_X$ and $S_\gamma$ denote fluences in the energy range of 2∼30 keV and 30∼400 keV and the error is in 1 sigma. As the ratio of fluences is $\log(S_x/S_\gamma)$ = -0.13, the GRB can be classified as an X-ray Rich GRB (Sakamoto et al. 2005).

The isotropic energy is calculated by:

$$E_{\rm iso} = \frac{4\pi D_L^2}{z+1} \int_{1/(z+1)}^{10^4/(z+1)} E\Phi dE \qquad (1)$$

where $D_L$ is a luminosity distance, $\Phi$ is a differential photon spectrum. We obtained $E_{\rm iso} = (0.707 \pm 0.04) \times 10^{52}$ ergs. In Figure 3, the peak energy at the source frame is plotted against the isotropic energy $E_{\rm iso}$ (a point labeled as "Total"). The relation for GRB 041006 obtained from the one component fit is slightly outside the Amati relation (Amati 2006 ).

Looking at the residual plot in the top panel of Figure 2, an additional soft component is apparently seen around 6 keV and a systematic excess is also seen around 50∼100 keV. Thus the total spectrum is fitted by a superposition of multiple basal functions. As a basal function, we considered a broken power law function and a blackbody radiation function. The results of the spectrum fitting for three three-component models are shown in Table 3. As a comparison the result of the two-component model and fitting by the Band function (Band 1993 ) and broken power law function are also shown in the table.

The Akaike's Information Criterion (AIC) is calculated for each model. AIC is a very widely used criterion to evaluate the goodness of the statistical model from both the goodness of fit and complexity of the model. AIC is defined by the following equation:

$$AIC = n \ln\left(\frac{\chi^2}{n}\right) + 2k, \qquad (2)$$

where $n$ is the number of data, $k$ is the number of free parameters to be estimated, and $\chi^2$ is the residual sum of squares from the estimated model. The AIC includes a penalty that is a increasing function of the number of estimated parameters, overfitting is discouraged, and thus this method enables to find the best model for the considered data, with minimum of free parameters. The model with the lower value of AIC is the one to be preferred.

The most preferable model is `bbody*2+bknp`. A model name is expressed by an algebraic expression of the name of a basal model. The second preferable model is `bknp*3`. The AIC values for the two models are 6.87 and 9.51 respectively.

The lowest AIC does not necessarily select the true model, and the degree of the preference is estimated by the AIC difference. The relation between the degree of the preference and the AIC difference ($\Delta_X$), however, depends on $n$ and the models to be compared. So we evaluate the confidence limit of AIC difference by carrying out a Monte Carlo simulation. The Monte Carlo simulation is performed by using `fakeit` command of XSPEC, which generates 1000 PHA samples based on the spectrum model to be tested. For each PHA sample, spectrum fit is performed for both the tested model and the model which gives the lowest AIC, then the AICs difference is calculated.

The left panel of Figure 4 shows a simulated distribution of the AIC difference $\Delta_{\texttt{bknp*3}} = AIC_{\texttt{bknp*3}} - AIC_{\texttt{bbody*2+bknp}}$. The simulation is performed according to the model spectrum `bknp*3` for which the model parameters are obtained from the fitting to the observed total spectrum. For each simulated PHA sample, model fitting is performed for both the `bknp*3` model and the model `bbody*2+bknp` which is the most preferred model. From this result the 90% confidence limit of $\Delta_{\texttt{bknp*3}}$ is estimated as 4.7 below which 90% of samples are included. The observed AIC difference for the model `bknp*3` is 2.64, so the model is acceptable in 90% C.L. In the case of Band spectrum model (right panel of the Figure 4), for 98% of the samples the AIC calculated for the Band model is smaller than the most preferred model `bbody*2+bknp`. The observed AIC difference is 13.68, so the Band model is rejected in higher than 98% C.L. All the three three-component models are acceptable in 90% C.L. The two-component model is rejected in 90% C.L.

As the time averaged spectrum of GRB 041006 is well represented by a superposition of the three components, we examined the $E_{p,src}$-$E_{\rm iso}$ relation for each one. The result is shown in Figure 3. The component with $E_p \sim 6$ $keV$ and $E_p \sim 20$ $keV$ are well within the Amati relation, and the component $E_p > 40$ $keV$ is just on the boundary of the 90% distribution width of the Amati relation. The $\log(S_x/S_\gamma)$ for the three components are: -0.2 for the component $E_p > 40$ $keV$, 0.1 for the component $E_p \sim 20$ $keV$, 0.3 for the component $E_p \sim 6$ $keV$, thus they are classified as XRR, XRF and XRF, respectively.

### *3.3. Time Resolved Spectrum Properties*

Time resolved spectrum analysis is performed for 12 independent time intervals, and also for some intermediate intervals which overlap with a part of one or two adjacent intervals to trance the spectrum evolution more closely.

We applied multi-component model in the spectrum fitting, where the model spectrum is represented as a superposition of arbitrary number of basal functions. The basal function considered here is a black body radiation function (`bbody`), a broken power law (`bknp`), and a single power law function (`pl`). The XSPEC built-in model is used for `bbody` and `pl`, for which the XSPEC model name are `bbody` and `powerlaw` respectively. For broken power law model, we used the following function to estimate the peak energy flux directly:

$$A(E) = K(E/E_p)^{-\alpha}, \qquad E \leq E_p \qquad (3)$$
$$K(E/E_p)^{-\beta}, \qquad E > E_p$$

The parameters $\alpha$ and $\beta$, which are lower and higher energy photon index, are restricted to the range of -2.0 $\sim$ 2.0 and 1.0 $\sim$ 5.0, respectively. The initial value of the break energy $E_p$ of `bknp` basal function is determined from local excess of the residual between the single `bknp` model and the observed data. The restriction to the break energy $E_p$ is applied so that the parameter converges around the initial value.

The fitting result for various combination of basal functions is summarized in Table 4. The fitting parameters for the lowest AIC model are shown in Table 5. The model spectrum giving the lowest AIC at each interval are shown in the Figure 6 and Figure 7. The expected number of components constituting the total spectrum is inferred from the number of local excess of in the residual plot for `bknp` model, and also from the light curves within the four energy bands. As an example, the case of interval 2c is shown in Figure 5. The spectrum is fitted with a single broken power law function, and $E_p$ is determined as $\sim$20 keV. Looking at the residual plot shown in the bottom of the figure, local excesses around 6 keV and 60 keV are seen. So the spectrum of interval 2c is expected to be constituted from three components which have peak energy of 6, 20, and 60 keV. In the case of interval 2b at least four components are expected from the light curves. One is the precursor component seen in the interval 1, which is expected to be present at the interval 2 if it is extrapolated smoothly. Two components corresponding to the two peaks seen in the 40$\sim$80 keV energy band and one component corresponding to the broad soft emission in the lowest energy band are also expected to be coexisting. So up to four components are examined for the interval 2b.

The model selection is carried out by examining the AIC difference, and 90% confidence limit of the AIC difference is calculated by performing a Monte Carlo simulation. By this statistical examination, single component models considered here are rejected for most of the intervals. The single component model is accepted only for the interval 1a, 4a, and 4b. For the other interval, the single component model considered here is rejected in 90% C.L. and the multi component models are preferred.

For most of the intervals, the null hypothesis probability is larger than 0.1. For interval 2b, however, the null hypothesis probability is at most 0.003. This is probably because unknown systematic error is involved in the data.

## 4. Discussion

The afterglow light curve in the optical R bands can be fitted by a broken power-law model and the break time is obtained to be $t_b = 0.16 \pm 0.04$ days (Stanek et al. 2005 ). Taking the $t_b$ as a jet break time and assuming homogeneous density profile around the GRB, jet opening angle $\theta$ is estimated by the following equation (Sari et al. 1999 ; Nava et al. 2006 ):

$$\theta = 0.161 \left(\frac{t_b}{1+z}\right)^{3/8} \left(\frac{n_0 \eta_\gamma}{E_{\rm iso,52}}\right)^{1/8}, \qquad (4)$$

where $n_0$ is an ambient particle density in cm$^{-3}$, $\eta_\gamma$ the radiation efficiency, and $E_{\rm iso,52} = E_{\rm iso}/$ ($10^{52}$ erg). Assuming $n_0 = 3$ and $\eta_\gamma = 0.2$, we obtain the jet opening angle of 3.4°. If the GRB is viewed on-axis, the collimation corrected total energy can be estimated by $E_\gamma = (1 - \cos\theta) E_{\rm iso}$. The corrected total energies for the three components are: $1.1^{+0.3}_{-0.2} \times 10^{49}$ erg for component of $E_p > 40$ keV, $0.36^{+0.37}_{-0.30} \times 10^{49}$ erg for component of $E_p \sim 20$ keV, and $0.036^{+0.358}_{-0.007} \times 10^{49}$ erg for component of $E_p \sim 6$ keV. Comparing them with the relation obtained by Ghirlanda et al. 2007 , we found that they don't follows the Ghirlanda relation. That is, the $E_p$ expected from the Ghirlanda relation are 13.2, 6.0 and 1.2 keV in the observer frame for the component $E_p > 40$ keV, $\sim$ 20 keV, and $\sim$ 6 keV, respectively. Considering 5% of uncertainty of the Ghirlanda relation, the observed $E_p$ are out of the relation.

Granot et al. 2005 showed that the afterglow light curve of GRB 041006 is naturally reproduced by an off-axis jet model, and an on-axis model is hard to reconcile the flat light curve observed at an early stage. If this is the case, the calculated $E_\gamma$ is underestimated and the discrepancy with the Ghirlanda relation could be explained.

Looking at the time evolution of $E_p$ obtained by the time resolved spectrum analysis as shown in Figure 8, we can identify seven components. Each of the identified components is interpolated with a solid line, and is given an identifier of A, $B_1$, $B_2$, $C_1$, $C_2$, $C_3$ or $C_4$.

The most preferred spectrum model for the component A at the interval 1a is the `bbody` model. The calculated emission radius is $4.35^{+1.35}_{-1.05} \times 10^6$ km, which corresponds to 6 solar radii and is a typical radius of a blue supergiant. The AIC difference for the second preferred `bknp` model is 3.31 and its 90% confidence limit is 4.9, so the `bknp` is also acceptable. The AIC difference for the power law spectrum with and without absorption (`wabs*pl` and `pl`) are larger than 8.9, and their 90% confidence limits are less than 0.3, so these model are rejected in 90% C.L.

In the case of the interval 1b, the acceptable models are `bbody*2`, `bbody+bknp` and `bknp*2`, all of which are a two-component model. None of the single component models considered here are not preferable and rejected in 90% C.L. So it is likely that the emission in the interval 1b is composed of two components (A and $B_1$). The

spectrum type of each component is not determined from this result, and it is either a black body or a broken power law function. Assuming that the component $B_1$ is black body radiation, the calculated emission radius is about one solar radius.

In the interval 2a $\sim$ 2d, the soft component A and $B_1$ are involved in all the acceptable models. The peak energies of the components are almost constant during the interval 1 and 2, and it is slightly decreasing with decay time $72.4\pm42.4$ sec for component A and $57.4\pm32.6$ sec for component $B_1$. Assuming that the components originate from thermal emission, the evolutions of the radiation radius are obtained, and they are shown in Figure 9 with the filled circles for the component A and with the open circles for the component $B_1$. The data point of the component $B_1$ are shifted by a factor of four. The data points of interval 1 and 2 are fitted with a linear function, and we obtained the apparent expansion velocity for the component A as $6.3\pm1.5\times10^5$ km/s, which is twice the speed of light. The superluminal motion is observed when the emitter is moving with the relativistic velocity toward an observer. The relation between the apparent expansion velocity $v$ and the velocity measured in the source frame $v'$ is given by:

$$v = \frac{v'}{(1+z)(1-\frac{v'}{c})}. \quad (5)$$

The expansion velocity at the source frame is $2.35\times10^5$ km/s, the corresponding Lorenz factor is 1.6. The apparent expansion rate for component $B_1$ is obtained as $1.1\times10^5$ km/s, and the velocity at the source frame is $1.2\times10^5$ km/s, which is half of the velocity of the component A.

If the component originates from the internal shock, according to the internal shock model by Zhang and Mészáros 2002 the following relation should be satisfied:

$$E_p \propto L^{1/2}\Gamma^{-2} \quad (6)$$

where $L$ is a luminosity and $\Gamma$ is a bulk Lorentz factor of the shock. When the spectrum shape is unchanged, the normalization constant $K$ of Eq. 4 is proportional to the luminosity. As the $\alpha$ and $\beta$ are not well constrained in the multi-component model due to the correlation of the parameters among the components, the luminosity is not well constrained. So we plotted the $E_p$-$K$ relation in Figure 10. If $\Gamma$ is constant and spectrum shape is not changed during the emission, it is expected that $E_p$ is proportional to $K^{1/2}$. No clear correlation is found for the component A (closed circle). For the component $B_1$ (closed triangle) the expected correlation is not found, instead it rather shows a negative correlation.

The higher energy components of the interval 2, $C_1$ and $C_2$, which corresponds to the two peaks seen in the light curve of 40$\sim$80 keV energy band, are resolved as a broken power law spectrum of which $E_p$ is around 50 $\sim$ 90 keV. If we assume that the $E_p$ decreases exponentially as seen in many GRBs, we can identify the correspondence among the $E_p$ as indicated in the Figure 8. The decay constant of the $E_p$ is $\sim$20 sec.

At the interval 3, the first precursor component seen in the interval 1a (component A) is not well resolved. The component $B_2$ has similar $E_p$ as that of the component $B_1$, but its $E_p$ is somehow systematically higher than the extrapolation of $B_1$. Assuming that the $B_2$ is a thermal emission, its radiation radius is calculated and shown in the Figure 9. The radiation radius is well below the extrapolation of those for $B_1$. The $E_p$-$K$ relation of $B_2$ is shown in the Figure 10, and it does not follow the relation given by Eq. 6.

The highly variable spectra whose emission peak varies from 100 keV to 40 keV are also resolved ($C_3$, $C_4$), and they correspond to the emissions seen in the light curve of the highest energy band. From the Figure 8, the $E_p$ of the components decrease as time exponentially with decay constant of $\sim$5 sec.

The $E_p$-$K$ relations for the $C_1$, $C_2$, $C_3$ and $C_4$ component are also shown in the Figure 10. Although the number of data points for each component are very few, the $E_p$-$K$ relations is satisfied except for two points. Both the exceptions are at the time intervals corresponding to the rising part of the component $C_1$ and $C_3$. At the rising part, due to the curvature effect the emission from a part of shock front that is moving toward us is dominated. After that the emission is averaged over the wider emission region, so the emission properties may change between the rising part and the following part.

In the interval 4a, the component $B_2$ is likely to remain and a black body spectrum of $T = 1$ keV or a broken power law spectrum with $E_p \sim 4$ keV is also likely to be present. In the interval 4b, the power law spectrum of photon index of 1.9 is the most preferable model, which is almost the same as the afterglow spectrum observed by Chandra.

## 5. Conclusion

We analyzed the time resolved spectra of GRB041006 and successfully resolved the components corresponding to the hard spikes and the soft broad bump observed in the multi-energy band light curves. The component may be divided into two classes. One is made of the component A, which has almost constant $E_p$ around 6 keV, and component $B_1$ and $B_2$ which have almost constant $E_p$ around 20 keV, The $E_p$ of this class gradually decreases in a time scale of 60$\sim$70 s. The spectrum type is well represented by a broken power law function or a black body radiation function. Assuming that the emission of this class is due to black body radiation, we derived the emission radius for the constituting components. The emission radii at the beginning of the emissions are $4\times10^6$ km for component A and $7\times10^5$ km for component $B_1$ and $B_2$. The expansion velocity at the source frame is also derived, which is 0.78 c and 0.4 c for component A and $B_1$, respectively. The emission radius of the component $B_2$ is almost constant.

$E_p$-Luminosity relation is examined for these components and compared with the prediction by the internal shock model. We used normalization constant $K$ of Eq. 4

instead of deriving the luminosity. According to the internal shock model by Zhang and Mészáros 2002 , the $E_p$ is proportional to $L^{1/2}$ if the bulk Lorentz factor of the shock is constant during the emission. We could not find such a correlation for the component A, $B_1$ and $B_2$.

Second class is made of the components whose $E_p$ is larger than the former class and shows relatively rapid decrease in a time scale of $5 \sim 20$ sec. The spectra are well represented by a broken power law function, and the $E_p$-K relation almost follows the relation expected for the internal shock origin. So they can be emissions caused by the internal shock.

We could not get to the conclusion about the origin of the soft component observed for GRB 041006, however, the difference of the time variability from that of the higher energy component is suggestive that it originates from different emission sites, such as acceleration by wider jet, emission by supernova shock breakout, or the emission from the photosphere of the fireball.

| energy range | T50(s) | T90(s) |
|---|---|---|
| 2 – 10 keV | 13.9±0.08 | 38.2±0.40 |
| 10 – 25 keV | 11.9±0.16 | 27.3±1.44 |
| 40 – 80 keV | 10.2±0.09 | 19.6±0.10 |
| 80 – 400 keV | 3.7 ±0.25 | 17.4±0.25 |

**Table 1.** Temporal properties, $T_{50}$ and $T_{90}$, of GRB 041006. The quoted errors corresponds to one sigma.

| time interval id | start (s) – end (s) |
|---|---|
| 1a | 2.5 – 6.0 |
| 1b | 6.0 – 12.5 |
| 2a | 12.5 – 16.5 |
| 2b | 16.5 – 19.5 |
| 2c | 19.5 – 23.0 |
| 2d | 23.0 – 27.5 |
| 3a | 27.5 – 29.5 |
| 3b | 29.5 – 31.0 |
| 3c | 31.0 – 34.0 |
| 3d | 34.0 – 38.0 |
| 4a | 38.0 – 42.5 |
| 4b | 42.5 – 60.0 |
| 2a' | 15.0 – 16.5 |
| 2c' | 22.0 – 24.0 |
| 3b' | 30.0 – 32.0 |
| 3c' | 33.0 – 35.0 |

**Table 2.** Time intervals used for time resolved spectrum analysis. The offset time is the trigger time 20041006_121808.63933.

| model | n | k | $\chi^2$ | p | AIC | $\Delta_X$ (90% limit) | |
|---|---|---|---|---|---|---|---|
| bbody*2+bknp | 83 | 8 | 74.35 | 0.499 | 6.87 | – | T=1.5,5.5,Ep=73 |
| bknp*3 | 83 | 12 | 69.70 | 0.521 | 9.51 | 2.64(4.7) | Ep=5,24,73 |
| bbody+bknp*2 | 83 | 10 | 73.75 | 0.453 | 10.19 | 3.32(4.1) | T=1.6,Ep=23,73 |
| bknp*2 | 83 | 8 | 77.80 | 0.390 | 10.63 | 3.76(<0) | Ep=5,24 |
| band | 83 | 4 | 96.55 | 0.087 | 20.55 | 13.68(<0) | Ep=38 |
| bknp | 83 | 4 | 111.19 | 0.010 | 32.27 | 25.40(<0) | Ep=22 |

**Table 3.** Result of the spectrum fitting to the time averaged spectrum. $n$ is the number of data used for the fitting, $k$ is the number of model parameter, $\chi^2$ is the chi-square of the fitting, $p$ is the null hypothesis probability, $AIC$ is the Akaike information criterion, $\Delta_X$ is the AIC difference between the corresponding model and the lowest AIC model. The number in the parentheses represents the 90% confidence limit of the AIC. The expected value of the fitting parameters are shown in the last column, where $T$ is the black body temperature in unit K, $E_p$ is the break energy of the `brknp` model. The unit of the parameter values are $keV$.

**Table 4.** Result of the spectrum model fitting to the time resolved spectra. $n$ is the number of data used for the fitting, $k$ is the number of model parameter, is the chi-square of the fitting, $p$ is the null hypothesis probability, $AIC$ is the Akaike information criterion, is the AIC difference between the corresponding model and the lowest AIC model. The number in the parentheses represents the 90% confidence limit of the AIC. The expected value of the fitting parameters are shown in the last column, where $T$ is the black body temperature in unit K, $E_p$ is the break energy of the `brknp` model measured in keV, $a$ is the power law photon index of the `pl` model, $nH$ is the column density measured in unit 10 22.

| interval | model | n | k | $\chi^2$ | p | AIC | $\Delta_X$(90%C.L.) | |
|---|---|---|---|---|---|---|---|---|
| 1a | bbody | 52 | 2 | 41.38 | 0.802 | -7.87 | – | T=2 |
| | bknp | 52 | 4 | 40.84 | 0.819 | -4.56 | 3.31(4.9) | Ep=8 |
| | wabs*pl | 52 | 3 | 47.26 | 0.543 | 1.03 | 8.90(0.3) | a=3.0,nH=16 |
| | pl | 52 | 2 | 56.57 | 0.243 | 8.38 | 16.25(0.0) | a=2.1 |
| 1b | bbody*2 | 52 | 4 | 36.27 | 0.893 | -10.74 | – | T=1.4,5.9 |
| | bbody+bknp | 52 | 6 | 35.92 | 0.857 | -7.24 | 3.50(5.1) | T=1.5,Ep=30 |
| | bknp*2 | 52 | 8 | 35.59 | 0.813 | -3.71 | 7.03(8.7) | Ep=6,30 |
| | bknp | 52 | 4 | 42.92 | 0.681 | -1.98 | 8.76(0.0) | Ep=6 |
| | bbody+pl | 52 | 6 | 49.93 | 0.320 | 5.89 | 16.63(0.0) | T=2.0,a=1.9 |
| | pl | 52 | 2 | 63.52 | 0.095 | 14.40 | 25.14(0.0) | p=1.9 |
| 2a | bbody*2+bknp | 80 | 8 | 59.34 | 0.857 | -7.91 | – | T=1.7,5.9,Ep=84 |
| | bbody+bknp*2 | 80 | 10 | 58.48 | 0.835 | -5.06 | 2.85(5.8) | T=2.7,Ep=23,84 |
| | bknp | 80 | 4 | 70.48 | 0.657 | -2.13 | 5.78(0.0) | Ep=25 |
| | bknp*2 | 80 | 8 | 64.77 | 0.715 | -0.90 | 7.01(4.6) | Ep=24,69 |
| | bknp*3 | 80 | 12 | 61.66 | 0.693 | 3.17 | 11.08(9.2) | Ep=5,24,67 |
| 2b OK | bbody*2+bknp | 80 | 8 | 104.91 | 0.007 | 37.69 | – | T=1.4,5.4,Ep=84 |
| OK | bbody*2+bknp*2 | 80 | 12 | 99.33 | 0.008 | 41.31 | 3.77(6.2) | T=1.4,5.5,Ep=50,85 |
| OK | bbody+bknp | 80 | 6 | 116.18 | 0.001 | 41.85 | 3.99(2.0) | T=1.5,Ep=21 |
| OK | bknp | 80 | 4 | 122.30 | 0.001 | 41.96 | 4.10(1.7) | Ep=23 |
| OK | bknp*2 | 80 | 8 | 111.59 | 0.002 | 42.63 | 4.77(4.1) | Ep=23,85 |
| OK | bknp*3 | 80 | 12 | 101.08 | 0.006 | 42.71 | 4.78(8.2) | Ep=5,22,85 |
| OK | bbody+bknp*2 | 80 | 10 | 106.05 | 0.004 | 42.55 | 5.22(5.5) | T=1.5,Ep=22,85 |
| 2c OK | bbody*2+bknp*2 | 73 | 12 | 49.53 | 0.853 | -4.32 | – | T=1.3,5.0,Ep=52,98 |
| OK | bbody*2+bknp | 73 | 8 | 56.66 | 0.760 | -2.50 | 1.67(<0) | T=1.3,5.0,Ep=53 |
| OK | bbody+bknp*2 | 73 | 10 | 56.61 | 0.702 | 1.44 | 5.76(0.2) | T=1.5,Ep=18,54 |
| OK | bknp*3 | 73 | 12 | 53.58 | 0.739 | 1.42 | 5.74(0.2) | Ep=5.5,18,74 |
| OK | bknp*2 | 73 | 8 | 62.24 | 0.574 | 4.36 | 8.68(0.06) | Ep=19,54 |
| OK | bbody+bknp | 73 | 6 | 66.70 | 0.488 | 5.41 | 9.73(<0) | T=4.7,Ep=55 |
| OK | bknp | 73 | 4 | 87.99 | 0.006 | 21.63 | 25.72(<0) | Ep=23 |
| 2d OK | bbody*2+bknp | 66 | 8 | 64.70 | 0.254 | 14.69 | —- | T=1.2,4.6,Ep=62 |
| OK | bbody+bknp | 66 | 6 | 72.12 | 0.136 | 17.85 | 3.16(0.9) | T=4.5,Ep=62 |
| | bknp*2 | 66 | 8 | 70.63 | 0.237 | 20.47 | 5.78(2.2) | Ep=17,36 |
| | bknp | 66 | 4 | 80.21 | 0.060 | 20.87 | 6.18(<0.0) | Ep=18 |
| | bbody+bknp*2 | 66 | 10 | 67.52 | 0.139 | 21.50 | 6.81(11.3) | T=1.6,Ep=17,60 |
| | bknp*3 | 66 | 12 | 66.93 | 0.111 | 24.92 | 10.23(15.2) | Ep=4,17,60 |
| 3a OK | bbody+bknp | 74 | 6 | 63.37 | 0.636 | 0.53 | – | T=6.8,Ep=96 |
| OK | bknp*2 | 74 | 8 | 63.72 | 0.557 | 4.93 | 4.40(4.9) | Ep=27,95 |
| OK | bbody+bknp*2 | 74 | 10 | 61.83 | 0.554 | 6.71 | 6.18(6.8) | T=6.0,Ep=50,92 |
| OK | bknp | 74 | 4 | 75.48 | 0.306 | 9.46 | 8.93(3.4) | Ep=36 |
| OK | bknp*3 | 74 | 12 | 62.21 | 0.469 | 11.15 | 10.62(11.8) | Ep=26,45,96 |
| 3b | bknp*2 | 84 | 8 | 80.20 | 0.349 | 12.11 | – | Ep=25,82 |
| OK | bknp*2+pl | 84 | 10 | 79.57 | 0.308 | 15.45 | 3.34(3.9) | Ep=26,84,a=1.3 |
| OK | bbody+bknp+pl | 84 | 8 | 83.64 | 0.257 | 15.64 | 3.53(3.0) | T=8,Ep=84,a=1.6 |
| OK | bknp*4 | 84 | 16 | 69.19 | 0.437 | 15.69 | 3.58(8.6) | Ep=6,10,21,84 |
| OK | bbody+bknp*2 | 84 | 10 | 80.17 | 0.292 | 16.08 | 3.97(4.0) | T=0.9,Ep=26,80 |
| OK | bbody+bknp | 84 | 6 | 85.91 | 0.413 | 17.89 | 5.78(<0) | T=8,Ep=83 |
| OK | bknp*3 | 84 | 12 | 79.88 | 0.245 | 19.78 | 7.67(7.2) | Ep=5,26,80 |
| | bknp | 84 | 4 | 107.35 | 0.022 | 28.60 | 16.49(<0) | Ep=67 |
| 3c OK | bknp*3 | 73 | 12 | 70.36 | 0.193 | 21.32 | – | Ep=26,44,120 |
| OK | bbody+bknp*3 | 73 | 14 | 67.43 | 0.211 | 22.20 | 0.88(4.5) | T=1.2,Ep=26,44,118 |
| OK | bknp*2 | 73 | 8 | 80.75 | 0.090 | 23.37 | 2.05(2.3) | Ep=44,130 |
| OK | bbody+bknp*2 | 73 | 10 | 78.07 | 0.096 | 24.90 | 3.58(1.3) | T=1.1,Ep=44,117 |

**Table 4.** (Continued.)

| interval | model | n | k | $\chi^2$ | p | AIC | $\Delta_X$(90%C.L.) | |
|---|---|---|---|---|---|---|---|---|
| OK | bknp*4 | 73 | 16 | 67.91 | 0.153 | 26.72 | 5.40(7.4) | Ep=6,26,44,119 |
| OK | bknp | 73 | 4 | 98.92 | 0.011 | 30.18 | 8.86(<0) | Ep=56 |
| 3d OK | bbody+bknp | 80 | 6 | 76.28 | 0.405 | 8.19 | – | T=6.1,Ep=72 |
| OK | bknp*2 | 80 | 8 | 77.40 | 0.310 | 13.36 | 5.17(5.8) | Ep=21,47 |
| OK | bknp | 80 | 4 | 86.42 | 0.194 | 14.18 | 5.99(<0) | Ep=24 |
| OK | bknp*3 | 80 | 12 | 74.91 | 0.264 | 18.74 | 10.55(13.6) | Ep=23,43,75 |
| 4a | bbody*2 | 66 | 4 | 59.23 | 0.576 | 0.86 | | T=1.2,5.2 |
| | bbody+bknp | 66 | 6 | 59.21 | 0.505 | 4.83 | – | T=1.2,Ep=24 |
| | bknp | 66 | 4 | 58.99 | 0.585 | 5.02 | 0.19(1.0) | Ep=26 |
| | bknp*2 | 66 | 8 | 57.44 | 0.496 | 6.84 | 2.01(8.4) | Ep=4,25 |
| | bbody+pl | 66 | 4 | 73.06 | 0.159 | 14.71 | 9.88(0.8) | T=4.7,a=2.3 |
| | pl | 66 | 2 | 100.05 | 0.003 | 31.45 | 26.62(0.0) | a=2.0 |
| 4b | pl | 52 | 2 | 47.31 | 0.582 | -0.92 | – | a=1.9 |
| | bbody+pl | 52 | 4 | 44.82 | 0.604 | 0.28 | 1.20(3.1) | T=1.5,a=1.8 |
| | bknp | 52 | 4 | 45.13 | 0.591 | 0.63 | 1.55(3.9) | Ep=4 |
| | pl+bknp | 52 | 4 | 45.01 | 0.596 | 0.63 | 1.55(3.0) | a=1.6,Ep=4 |
| | bknp*2 | 52 | 8 | 43.23 | 0.668 | 6.40 | 7.32(11.6) | Ep=9,20 |
| | bbody | 52 | 2 | 69.71 | 0.022 | 19.24 | 20.16(0.0) | T=1.7 |

| interval | component | parameter | | | |
|---|---|---|---|---|---|
| 1a | 1 | $kT = 1.92^{+0.30}_{-0.27}$ | $R = 4.35^{+1.35}_{-1.05}$ | | |
| 1b | 1 | $kT = 1.44^{+0.18}_{-0.17}$ | $R = 8.92^{+2.18}_{-1.62}$ | | |
| | 2 | $kT = 5.94^{+1.26}_{-1.09}$ | $R = 0.60^{+0.28}_{-0.19}$ | | |
| 2a | 1 | $kT = 1.82^{+1.47}_{-0.64}$ | $R = 5.04^{+8.46}_{-3.49}$ | | |
| | 2 | $kT = 6.16^{+2.41}_{-1.60}$ | $R = 0.738^{+0.662}_{-0.383}$ | | |
| | 3 | $E_p = 83.5^{+13.6}_{-16.4}$ | $\alpha = 1.46^{+0.20}_{-0.53}$ | $\beta = 5.00^{+0.00}_{-1.81}$ | $K = 48.4^{+11.7}_{-13.1}$ |
| 2b | 1 | $kT = 1.39^{+0.24}_{-0.16}$ | $R = 14.3^{+5.10}_{-5.58}$ | | |
| | 2 | $kT = 5.39^{+0.55}_{-0.47}$ | $R = 1.59^{+0.33}_{-0.34}$ | | |
| | 3 | $E_p = 84.4^{+8.8}_{-34.9}$ | $\alpha = 1.23^{+0.33}_{-0.79}$ | $\beta = 5.00^{+0.00}_{-0.95}$ | $K = 58.7^{+12.7}_{-13.1}$ |
| 2c | 1 | $kT = 1.34^{+0.18}_{-0.08}$ | $R = 16.6^{+2.9}_{-2.7}$ | | |
| | 2 | $kT = 5.01^{+1.09}_{-0.46}$ | $R = 2.19^{+0.28}_{-0.68}$ | | |
| | 3 | $E_p = 52.3^{+5.0}_{-7.6}$ | $\alpha = 0.24^{+1.01}_{-2.24}$ | $\beta = 5.00^{+0.00}_{-1.90}$ | $K = 97.9^{+35.1}_{-40.5}$ |
| | 4 | $E_p = 95.5^{+13.0}_{-9.7}$ | $\alpha = 0.06^{+1.37}_{-2.06}$ | $\beta = 5.00^{+0.00}_{-1.44}$ | $K = 78.4^{+19.2}_{-49.7}$ |
| 2d | 1 | $kT = 1.28^{+0.48}_{-0.19}$ | $R = 14.1^{+5.20}_{-8.54}$ | | |
| | 2 | $kT = 4.65^{+0.42}_{-0.34}$ | $R = 2.25^{+0.38}_{-0.45}$ | | |
| | 3 | $E_p = 62.1^{+7.1}_{-11.5}$ | $\alpha = 1.23^{+0.33}_{-0.53}$ | $\beta = 5.00^{+0.00}_{-0.82}$ | $K = 54.1^{+6.0}_{-10.7}$ |
| 3a | 1 | $kT = 6.72^{+1.23}_{-1.08}$ | $R = 0.842^{+0.268}_{-0.212}$ | | |
| | 2 | $E_p = 95.7^{+9.3}_{-14.9}$ | $\alpha = 1.50^{+0.07}_{-0.07}$ | $\beta = 5.00^{+0.00}_{-1.52}$ | $K = 106.8^{+17.4}_{-17.3}$ |
| 3b | 1 | $E_p = 25.4^{+3.0}_{-5.3}$ | $\alpha = -0.86^{+1.19}_{-1.14}$ | $\beta = 5.00^{+0.00}_{-2.63}$ | $K = 68.3^{+20.9}_{-22.1}$ |
| | 2 | $E_p = 80.3^{+5.2}_{-7.8}$ | $\alpha = 1.04^{+0.15}_{-0.38}$ | $\beta = 3.22^{+0.58}_{-0.39}$ | $K = 383.0^{+40.8}_{-134.9}$ |
| 3c | 1 | $E_p = 26.0^{+2.1}_{-3.2}$ | $\alpha = -0.12^{+0.74}_{-1.88}$ | $\beta = 5.00^{+0.00}_{-2.33}$ | $K = 69.8^{+12.0}_{-43.5}$ |
| | 2 | $E_p = 44.2^{+11.9}_{-3.5}$ | $\alpha = -2.00^{+2.45}_{-0.00}$ | $\beta = 2.65^{+2.25}_{-0.36}$ | $K = 115.9^{+25.4}_{-57.7}$ |
| | 3 | $E_p = 120.2^{+9.3}_{-6.9}$ | $\alpha = 1.33^{+0.30}_{-0.29}$ | $\beta = 5.00^{+0.00}_{-1.38}$ | $K = 159.0^{+96.6}_{-24.2}$ |
| 3d | 1 | $kT = 6.08^{+0.35}_{-0.72}$ | $R = 0.992^{+0.208}_{-0.167}$ | | |
| | 2 | $E_p = 71.7^{+14.1}_{-29.6}$ | $\alpha = 1.38^{+0.11}_{-0.09}$ | $\beta = 4.32^{+0.68}_{-1.53}$ | $K = 55.9^{+11.7}_{-12.0}$ |
| 4a | 1 | $kT = 1.24^{+0.18}_{-0.16}$ | $R = 12.4^{+3.7}_{-2.7}$ | | |
| | 2 | $kT = 4.45^{+0.81}_{-0.71}$ | $R = 0.94^{+0.30}_{-0.23}$ | | |
| 4b | 1 | $\alpha = 2.03^{+0.17}_{-0.15}$ | $K = 5.14^{+1.78}_{-1.30}$ | | |

**Table 5.** Fitting parameters for the most preferred models, that is the model that gives the lowest AIC. $kT$ and $R$ is temperature and radiation radius of black-body radiation model, respectively. $E_p$, $\alpha$, $\beta$, $K$ is peak energy, low energy photon index, high energy photon index, and normalization constant defined in Eq. 4

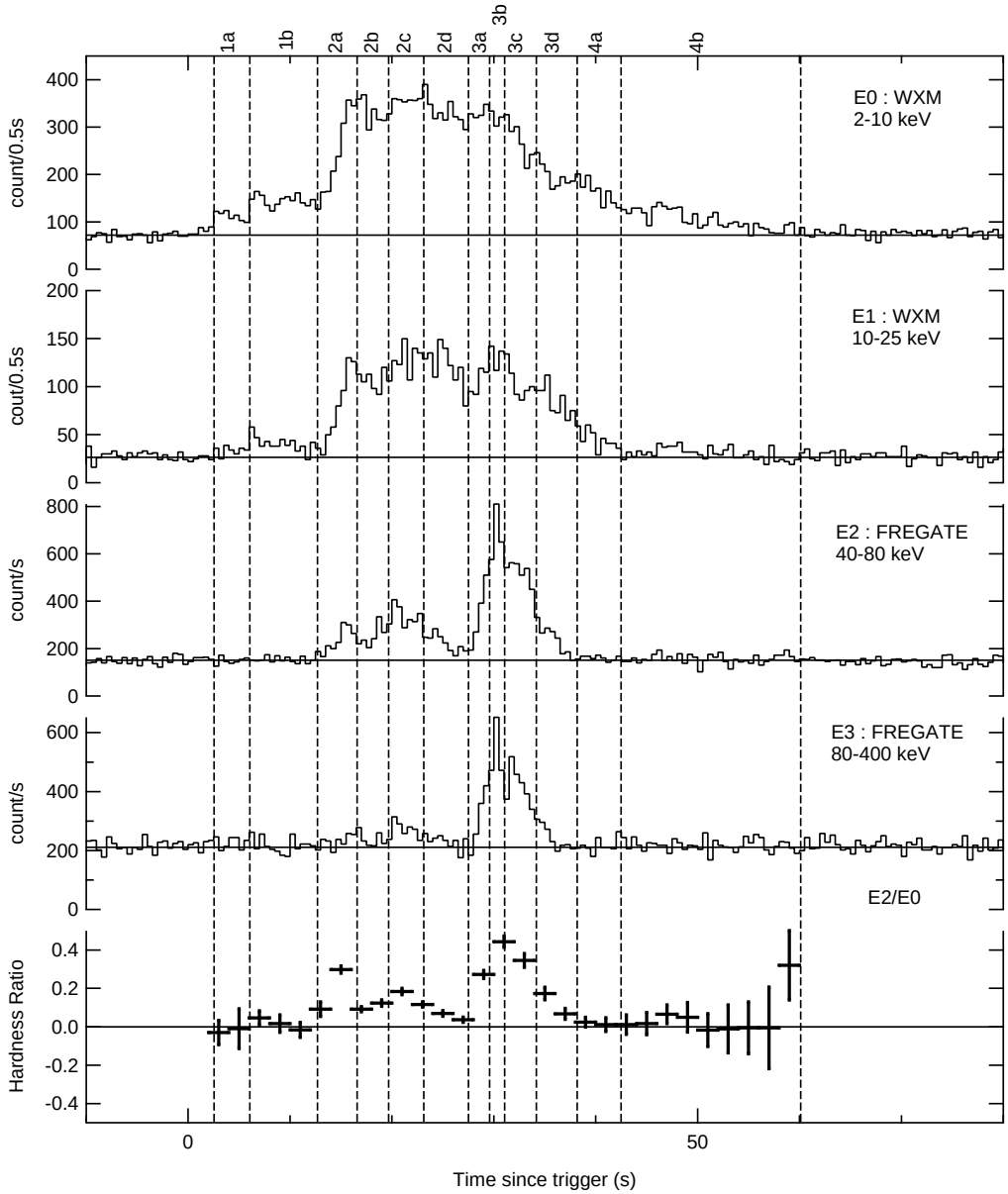


**Fig. 1.** Light curves of GRB041006 for each energy band and hardness ratio. From top to bottom, 2–10 keV, 10–25 keV, 40–80 keV, and 80–400 keV. The hardness ratio is calculated by dividing the count rate in 40∼80 keV by the count rate in 2∼10 keV. The vertical lines represents the boundary of time intervals for time resolved spectrum analysis.

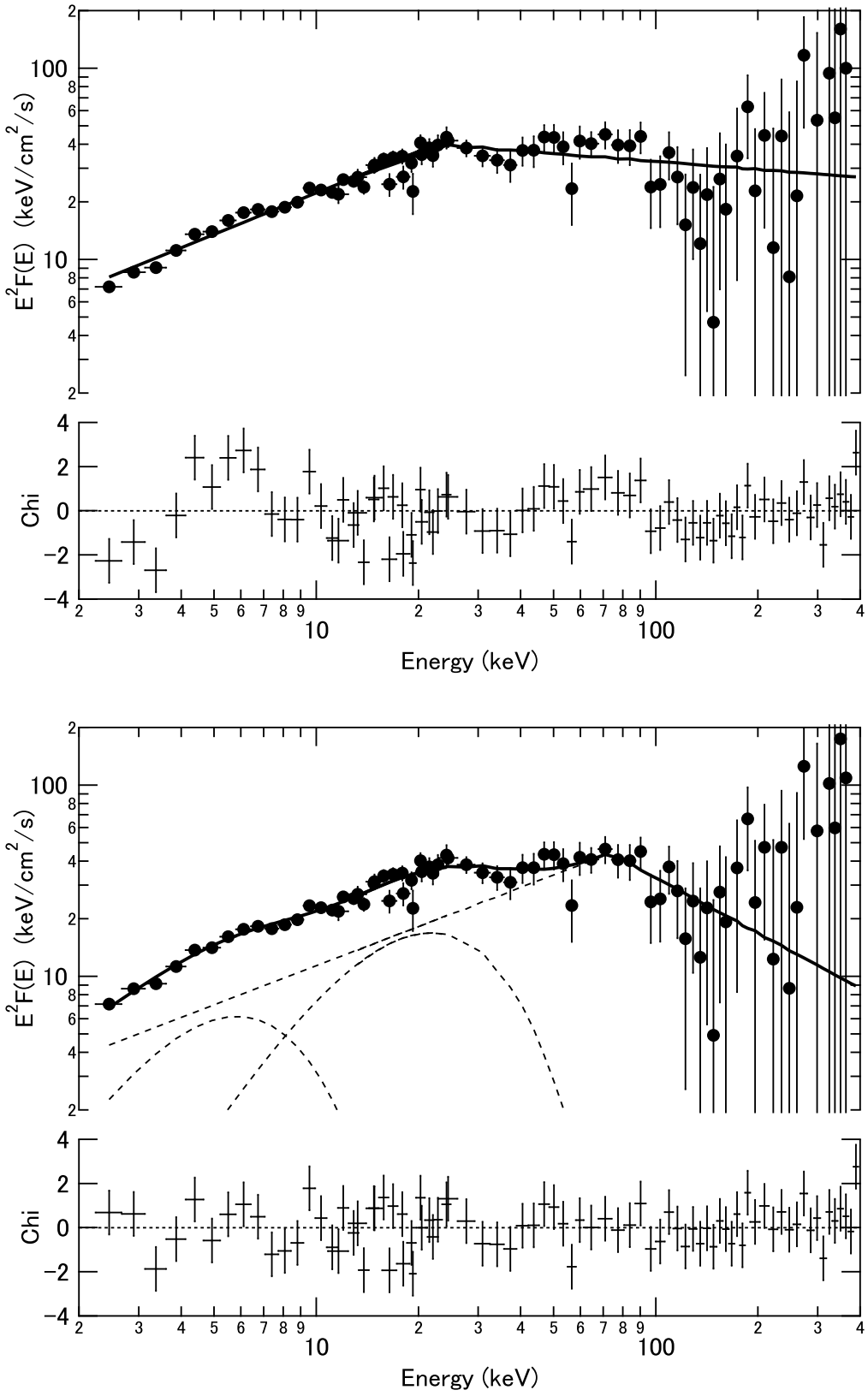


**Fig. 2.** Time averaged unfolded spectrum expressed in $\nu f_\nu$. Top: Fitting result for the broken power law model. Bottom: Fitting result for the three-component model represented by a superposition of the three broken power law functions.

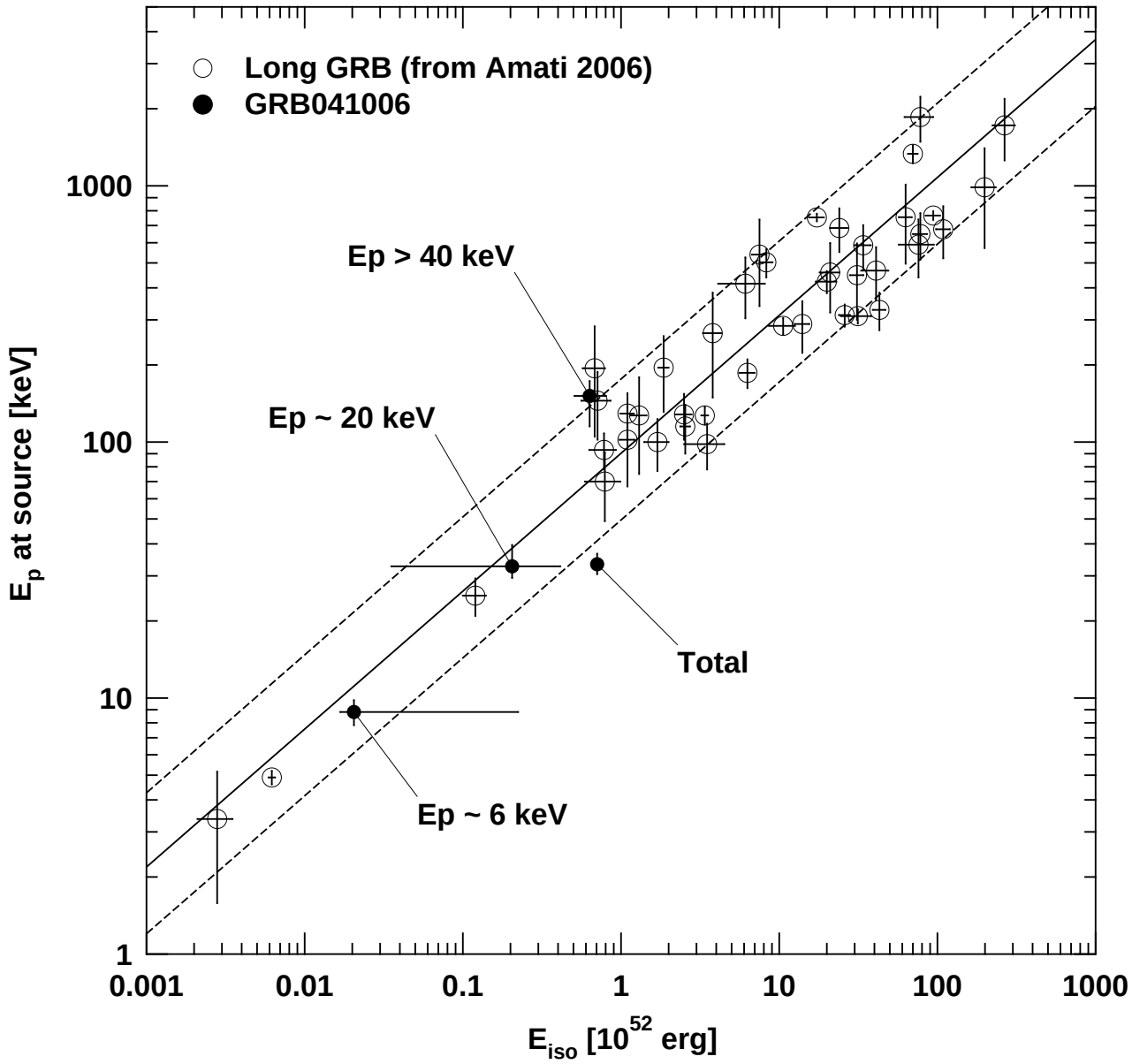


**Fig. 3.** $E_{\rm p,src}$-$E_{\rm iso}$ relation for long GRBs. The open circles represent the long GRBs compiled by Amati 2006 . The solid circles represent GRB 041006. The solid circles labeled as "Total" is derived from a single broken power model. The other solid circles are derived from a three-component model. The solid line represent the average relation derived from all the point of the open circles, the dashed lines represent lower and upper boundary which are parallel to the average relation and contain 90% of the circle points.

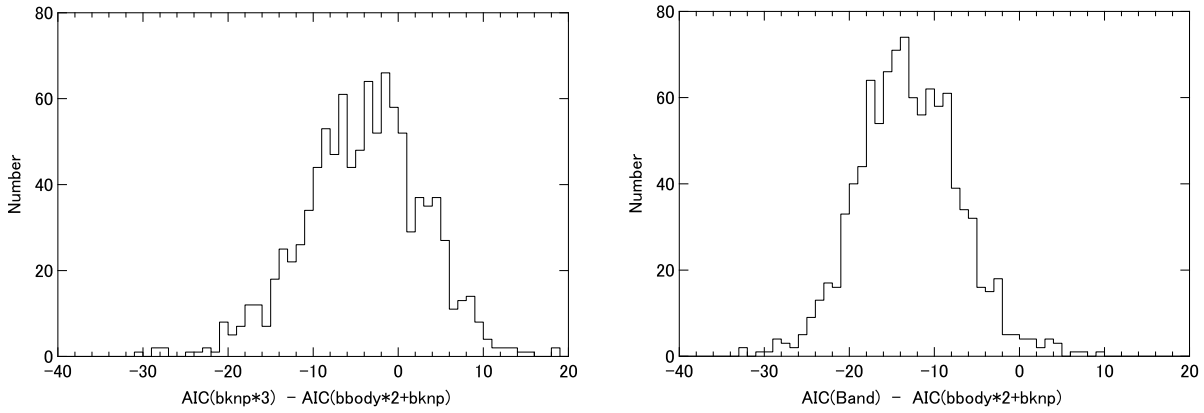


**Fig. 4.** Left: Simulated distribution of AIC differences between the `bknp*3` and `bbody*2+bknp` model (left). Simulation is performed according to the `bknp*3` model, and then model fitting to the simulated data is carried out for both the models. The `bbody*2+bknp` model is the most preferable model for the time integrated spectrum. The AICs for the two model are calculated for each simulated spectrum. The fraction of events with $\Delta_{AIC} > 0$ corresponds to the probability for wrong model selection. Right: Same plot for Band model.

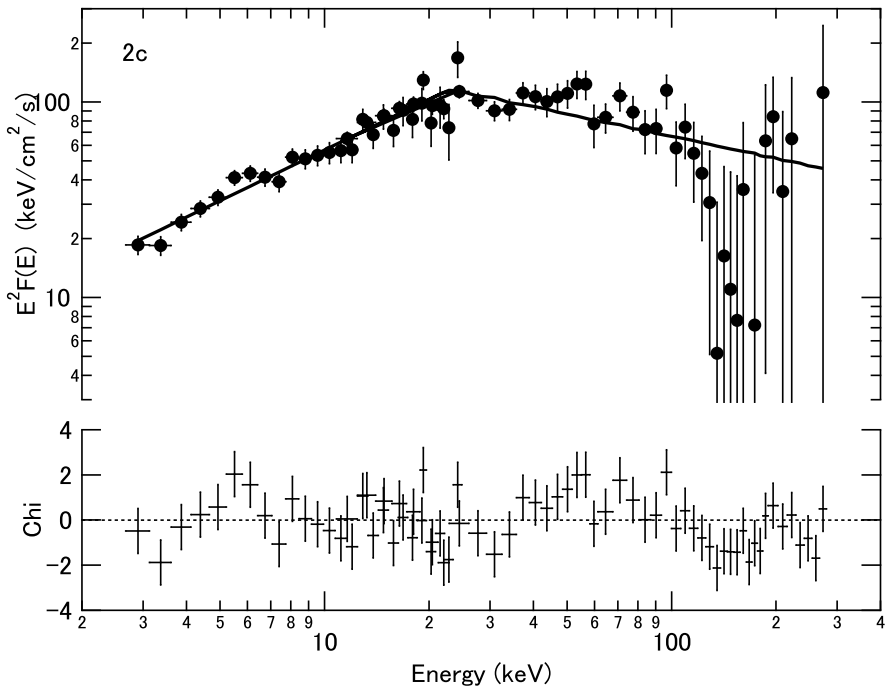


**Fig. 5.** An example of spectrum fitting for the interval 2c, where single-component model is used.

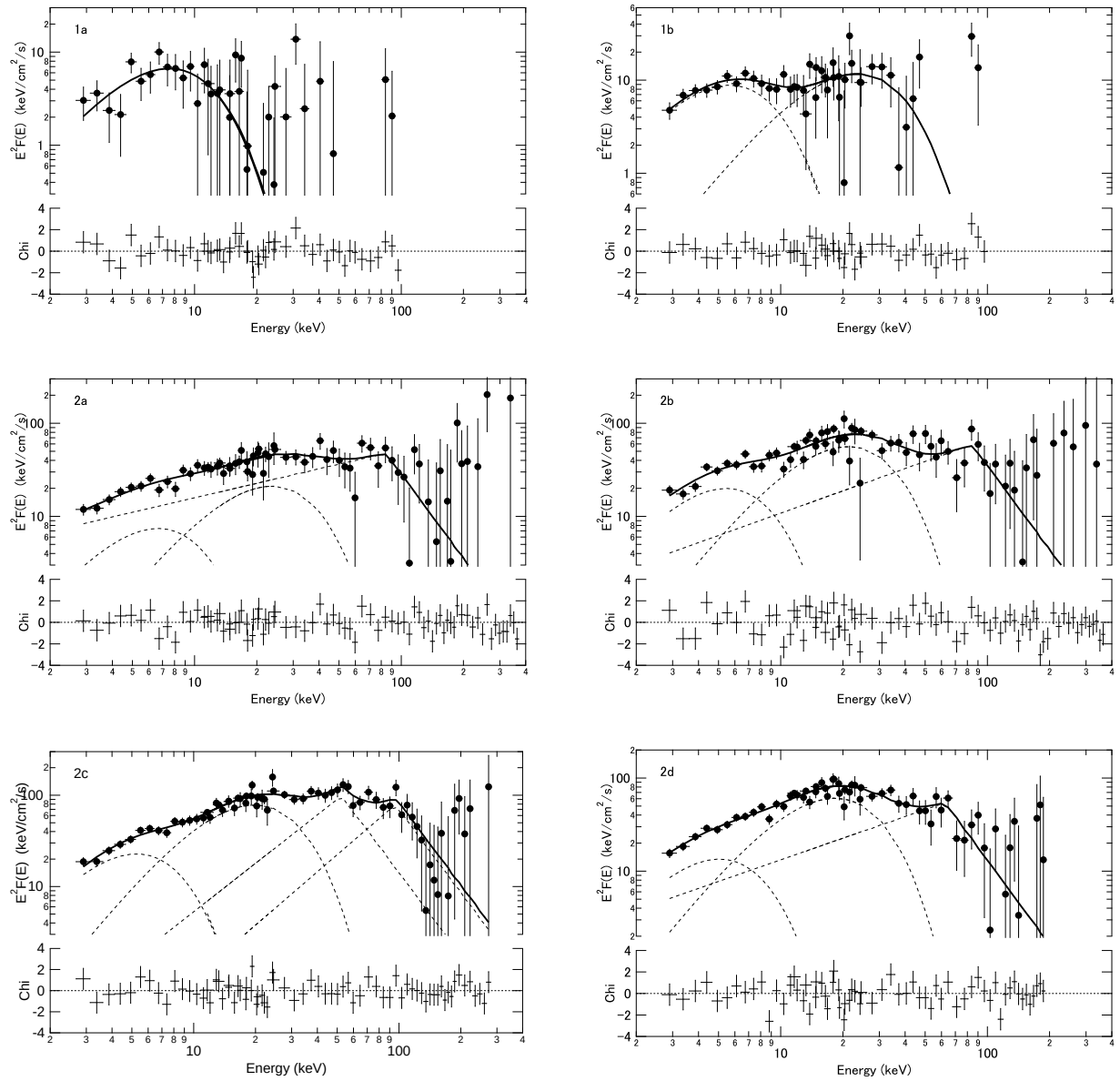


**Fig. 6.** Time resolved unfolded spectrum for interval 1 and 2. The residual between the observation and the model is also shown at the bottom panel of each figure. The spectrum is expressed in $\nu f_\nu$. The most preferable model spectra are plotted as a solid line (total) and dashed lines (basal function).

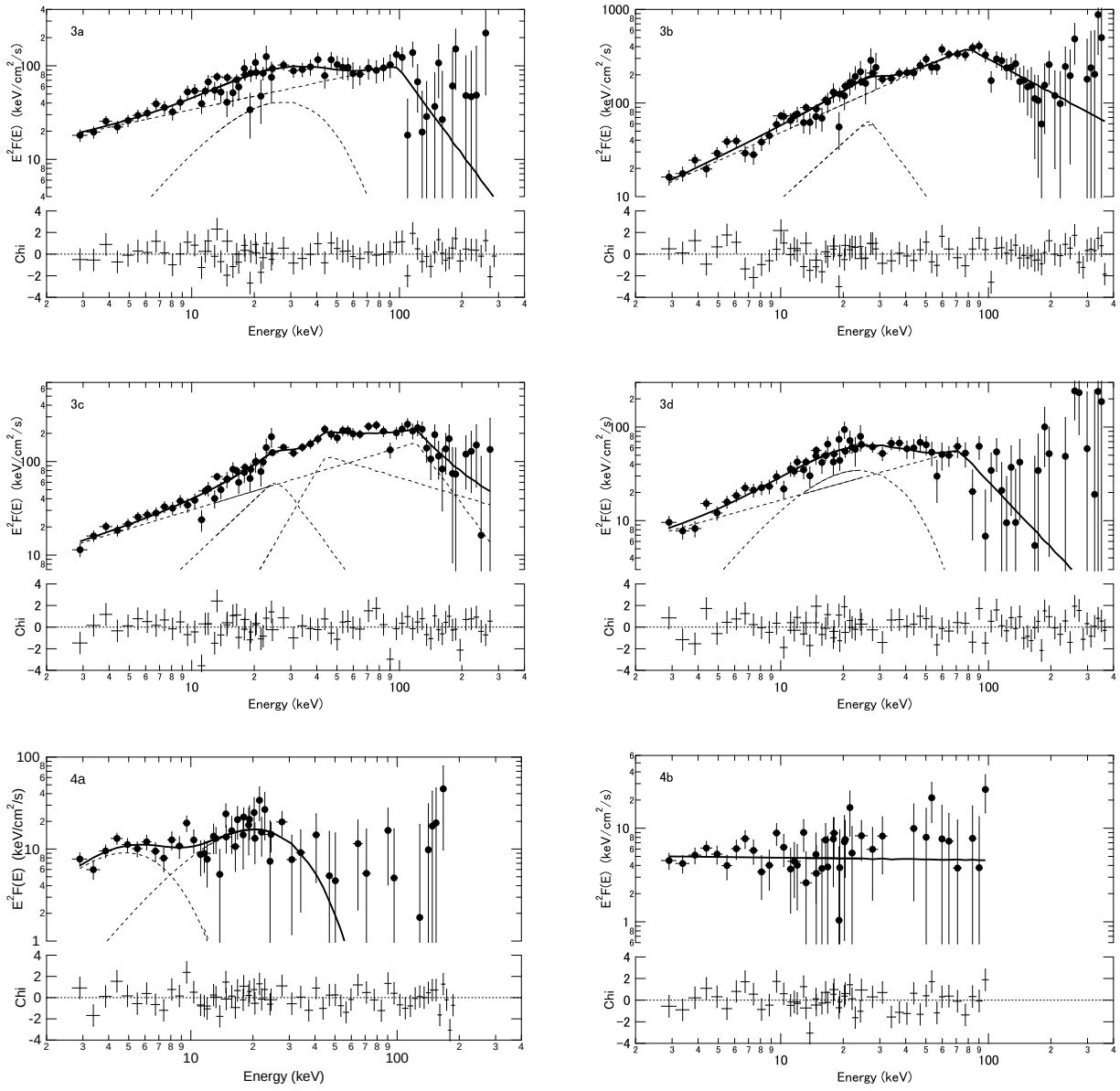


**Fig. 7.** Time resolved unfolded spectrum for interval 3 and 4.

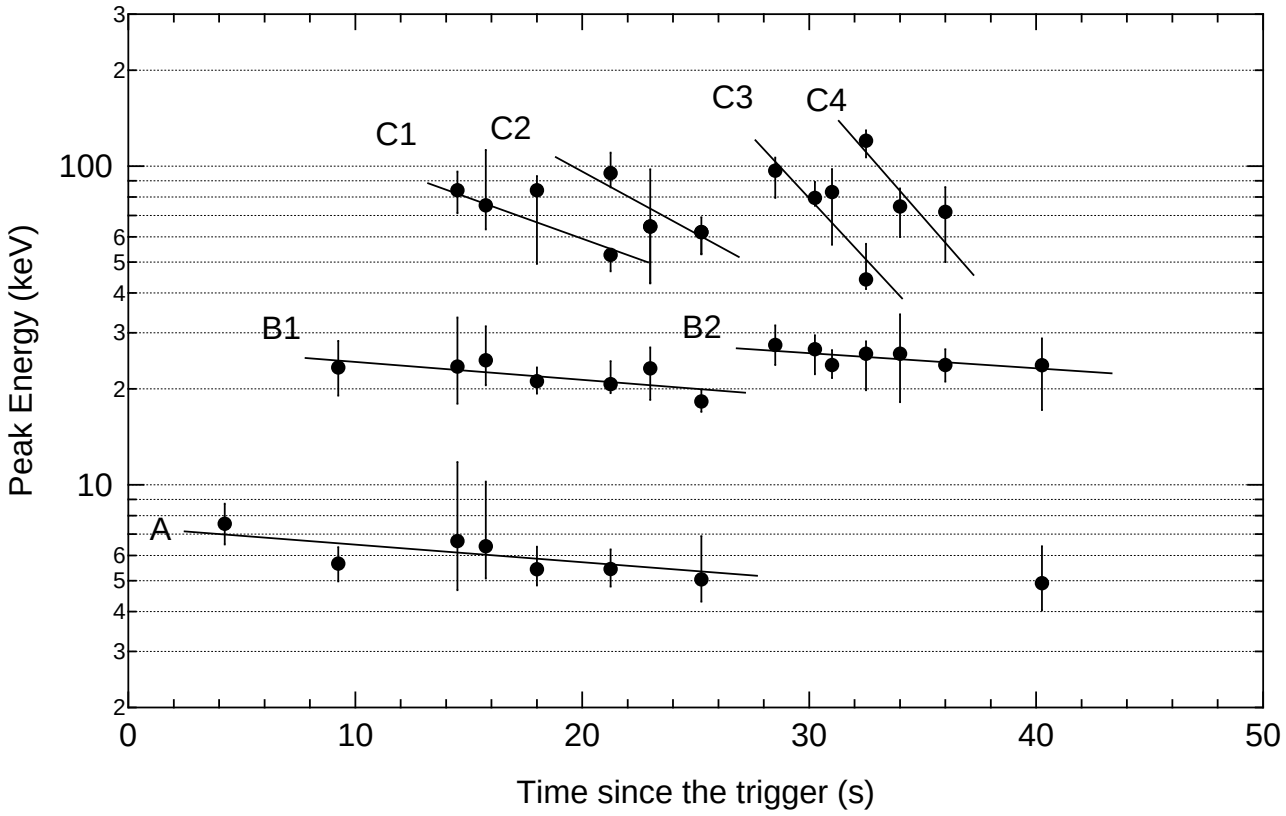


**Fig. 8.** Peak energy calculated for each interval by fitting the data with multi-component model. The points which are inferred to belong to the identical component are interpolated with a line. The vertical error bar corresponds to an error in 90% C.L.

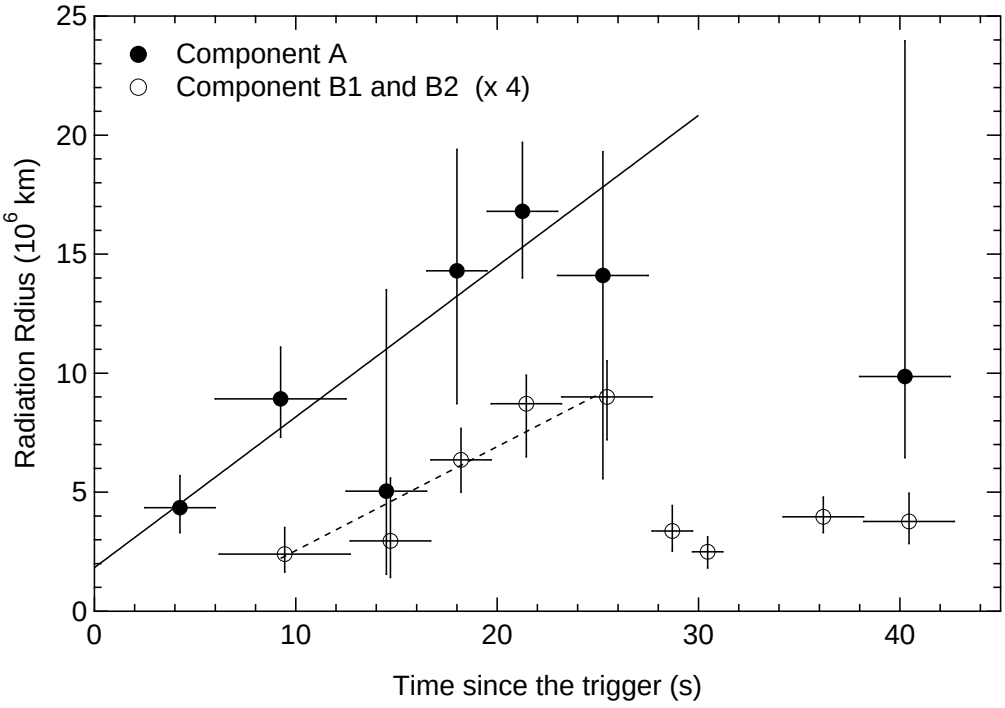


**Fig. 9.** Evolution of the radiation radius of the black body components. The filled circles represent the component A of the Figure 8. The open circles represent the component $B_1$ and $B_2$, for which the radius is multiplied by four. The solid and dashed line represent the linear fit to the data of interval 1 and 2.

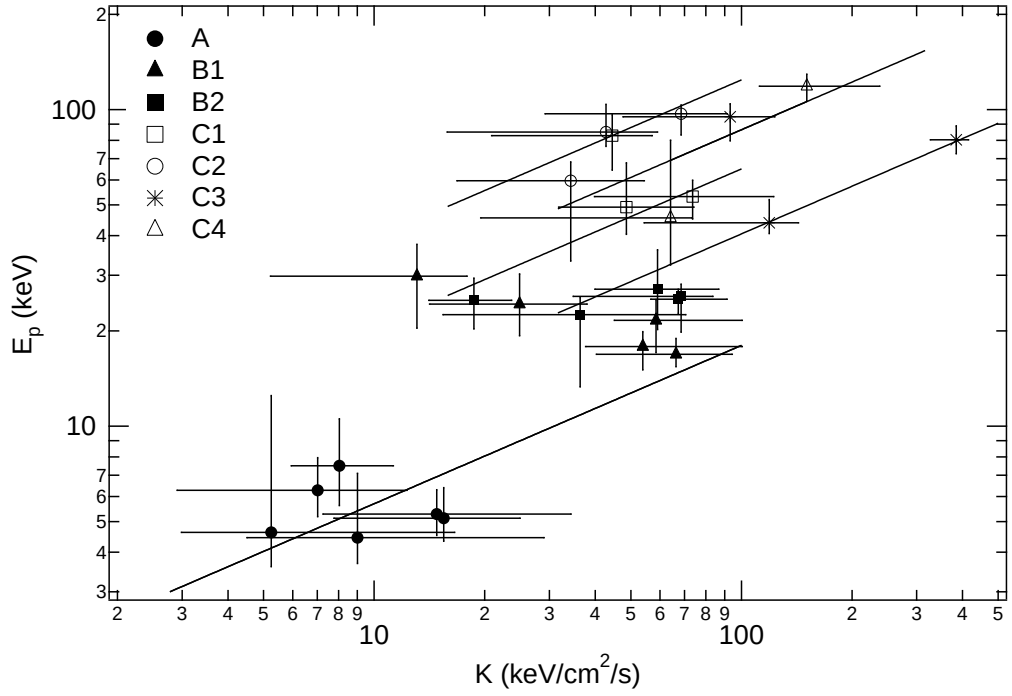


**Fig. 10.** The relation between $E_p$ and $K$ of Eq. 4 for each component. Solid lines represent the relation $E_p \propto K^{0.5}$.

## References

T. Murakami et al. 1991, Nature, **350**, 592
L. Piro et al. 2005, ApJ, **623**, 314
S. B. Cenko et al. 2006, ApJ, **652**, 490
P. Romona El Ac. 2006, A&A, **456**, 917
K. L. Page et al. 2007, ApJ, accepted (astro-ph 0704.1609)
B. Paczynsky 1986, ApJ, **308**, L43
F. Daigne & R. Mochkovitch 2002, MNRAS, **336**, 1271
E. Ramirez-Ruiz, A. I. MacFadyen, D. Lazzati 2002, MNRAS, **331**, 197
E. Waxman, P. Mészáros, 2003, ApJ, **584**, 390
H. Umeda et al. 2005, ApJ, **633** L17
L. Vetere et al. 2006, A&A, **447**, 499
L. Borgonovo et al. 2007, A&A, **465**, 765
D. Lazzati 2005, MNRAS, **357**, 722
R. Vanderspek et al. 2004, ApJ, **617**, 1251
Y. Urata et al. 2007 ApJ, **655**, L81
A. M. Soderberg et al. 2005 ApJ, **636**, 391
N. R. Butler et al. 2005, ApJ, **629**, 908
T. Sakamoto et al. 2005, ApJ, **629**, 311
Y. Shirasaki et al. 2003, PASJ, **55**, 1033
J.-L. Atteia et al. 2003, in Gamma-Ray Burst and Afterglow Astronomy, ed. G. R. Ricker & R. Vanderspek (Melville: AIP), 662, 17
K. Z. Stanek et al. 2005, ApJ, **626**, L5
R. Sari, T. Piran, & J. Halpern 1999, ApJ, **519**, L17
R. A. Chevalier & Z.-Y. Li 2000, ApJ, **536**, 195
L. Nava et al, 2006, A&A, **450**, 471
G. Ghirlanda et al. 2007, A&A, **466**, 127
J. Granot, E Ramirez-Ruiz, & Rosalba Perna 2005, ApJ, 630, 1003.
A. M. Soderberg et al. 2005, ApJ, **636**, 391
M. Galassi et al 2004, GCN notice #2770
G. da Costa, N. Noel and P.A. Price 2004, GCN notice #2765
D. Fugazza et al. 2004, GCN notice #2782
P. A. Price et al. 2004, GCN notice #2791
A. M. Soderberg et al. 2004, GCN notice #2787
I. Bikmaev et al. 2004, GCN notice #2826
A. Garg et al. 2004, GCN notice #2829
D. Band et al. 1993, ApJ, **413**, 281
K. A. Arnaud 1996, ASP Conf. Ser. 101: Astronomical Data Analysis Software and Systems V, 101, 17
L. Amati 2006, MNRAS, **372**, 233
B. Zhang, & P. Mészáros 2002, ApJ, **581**, 1236